Cytotoxic Effects of Gold Nanoparticles: A Multiparametric Study

Stefaan J. Soenen,[†] Bella Manshian,[‡] José Maria Montenegro,[§] Faheem Amin,[§] Björn Meermann,[⊥] Toke Thiron,[∥] Maria Cornelissen,[∥] Frank Vanhaecke,[⊥] Shareen Doak,[‡] Wolfgang J. Parak,[§] Stefaan De Smedt,[†,*] and Kevin Braeckmans[†]

[†]Lab of General Biochemistry and Physical Pharmacy, Faculty of Pharmaceutical Sciences, Ghent University, B-9000 Ghent, Belgium, [‡]DNA Damage Group, Institute of Life Science, Swansea University, Singleton Park, Swansea, U.K., [§]Biophotonics Group and WZMW, Philipps University of Marburg, D-35032 Marburg, Germany, [⊥]Department of Analytical Chemistry, Ghent University, B-9000 Ghent, Belgium, and [∥]Lab of Histology, Faculty of Medicine, Ghent University, B-9000 Ghent, Belgium

ABSTRACT The *in vitro* labeling of therapeutic cells with nanoparticles (NPs) is becoming more and more common, but concerns about the possible effects of the NPs on the cultured cells are also increasing. In the present work, we evaluate the effects of poly(methacrylic acid)-coated 4 nm diameter Au NPs on a variety of sensitive and therapeutically interesting cell types (C17.2 neural progenitor cells, human umbilical vein endothelial cells, and PC12 rat pheochromocytoma cells) using a multiparametric approach. Using various NP concentrations and incubation times, we performed a stepwise analysis of the NP effects on cell viability, reactive oxygen species, cell morphology, cytoskeleton architecture, and cell functionality. The data show that higher NP concentrations (200 nM) reduce cell viability mostly through induction of reactive oxygen species, which was significantly induced at concentrations of 50 nM Au NPs or higher. At these concentrations, both actin and tubulin cytoskeleton were deformed and resulted in reduced cell proliferation and cellular differentiation. In terms of cell functionality, the NPs significantly impeded neurite outgrowth of PC12 cells up to 20 nM concentrations. At 10 nM, no significant effects on any cellular parameter could be observed. These data highlight the importance of using multiple assays to cover the broad spectrum of cell–NP interactions and to determine safe NP concentrations and put forward the described protocol as a possible template for future cell–NP interaction studies under comparable and standardized conditions.

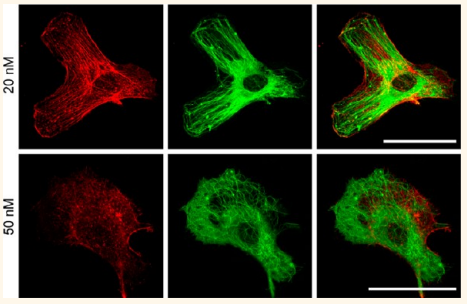

KEYWORDS: gold nanoparticles · nanotoxicology · cytotoxicity · biocompatibility · nanoparticle–cell interaction

Advances in nanotechnology are paving the way for future biomedical applications of nanosized materials.[1−5] To date, the number of novel biomedical applications are very limited, in contrast to the vast number of nanotechnological developments.[2] The translation of nanotechnological improvements into the field of biomedicine is made difficult by several factors, one of the most important being the current incomplete knowledge on cell–nanoparticle (NP) interactions.[6] In order to address this issue, the field of nanotoxicology has recently gained a lot of interest. The amount of toxicological data produced is steadily increasing, hereby enhancing our knowledge of cell–NP interactions. However, the wide variety of cell labeling conditions and physicochemical properties of the NPs (size, applied coating, purity, surface functionalization, *etc.*) and the large range of different cell types, each with their specific characteristics, have given rise to quite a substantial amount of disparate data and conclusions. Recently, more attention has been put toward standardization of toxicity testing and trying to prepare the field of nanotoxicity research in view of the ever-increasing interest in nanotechnology.

One type of NP that has been given a lot of attention in the development of biomedical applications such as drug and gene delivery, whole body noninvasive imaging, and hyperthermia cancer therapy are Au NPs.[7−9] The wide interest in Au NPs stems from a broad variety of enticing properties that Au NPs possess, such as: (1) high chemical stability, (2) narrow size control during synthesis, (3) easy surface functionalization with amines or thiols, and (4) the high biocompatibility of bulk gold.[10] Due to the chemical stability of bulk gold and its low toxicity, Au NPs were initially expected to be well suited for biomedical purposes and not to elicit any cytotoxic effects at concentrations relevant for the envisaged applications. Recently, however, this presumption had to be reconsidered, as multiple studies have been reported describing damaging effects of nanosized Au.[11−13] Unfortunately, these studies suffer from a lack of standardization, and therefore no consensus has thus far been reached on the cytotoxic potential of Au NPs. Several key findings

* Address correspondence to Stefaan.DeSmedt@ugent.be.

Received for review November 1, 2011 and accepted June 2, 2012.

Published online June 03, 2012
10.1021/nn301714n

that have independently been described by multiple laboratories can however be considered as important key points to consider when exposing biological specimens to Au NPs: (1) Size: the smaller the particles, the higher the surface area to volume ratio, which enables a larger extent of interaction of the NPs with cellular or intracellular components. Also, smaller NPs are more likely to reach intracellular locations such as the nucleus, which cannot be reached by larger sized materials. Therefore, smaller sized particles are often considered as more dangerous.[14] However, as previous work has shown that Au NPs show a size-dependent cellular uptake with an optimal size of approximately 50 nm,[15,16] and as toxic effects exerted by NPs are linked to their cellular uptake levels, the influence of size may not be so straightforward. (2) Coating: either during synthesis or for stability in physiological media, coating agents are frequently applied, such as cetyltrimethylammonium bromide (CTAB), a cationic surfactant. CTAB has been shown to desorb from the Au NP surface, however, and thereby induce cell death irrespective of the actual effects of the Au NPs themselves. Using polymer-coated particles, the toxic effects of the Au NPs were greatly reduced.[17−19] In order to fully unveil the toxicological profile of Au NPs, there is a high need for (1) standardized protocols for multiparametric analysis of cell−NP interactions at different time points and NP concentrations, (2) reference materials to allow easy comparison of NP toxicity levels, (3) a set of well-suited cell types that could be used for proper toxicity testing, and (4) the definition of key parameters, which are essential to address.

As many applications of nanomaterials rely on the *in vitro* labeling of cells followed by transplantation of the marked cells *in vivo*, the effects of the particles on cultured cells must be carefully analyzed in order to promote any further clinical translation of proof of concept studies. An interesting question that remains unanswered in the field of nanotoxicology today is whether nanosized materials as such pose any specific threats solely due to their size and thus irrespective of the specific type of core material. To answer this question, standard toxicity assays as used for drug screening have not been sufficient and sometimes cannot be used at all due to NP interference with the assay readout.[20] Recently, we proposed a standardized strategy that could serve as a template for any *in vitro* NP toxicity study and that addressed all points described above.[21] In the present work, we looked into the effects of 4 nm diameter poly(methacrylic acid) (PMA)-coated Au NPs on cell viability, physiology, and functionality. To this end, we employed the previously proposed strategy that entailed the use of multiple cell types (C17.2 murine neural progenitor cells, PC12 rat pheochromocytoma cells, and primary human umbilical vein endothelial cells (HUVECs)), multiple NP concentrations, and time points in order to cover a large spectrum of cell−NP interactions. A step by step approach is then followed, where the following points were studied: cell viability, reactive oxygen species (ROS), cell morphology and architecture of cell cytoskeleton, and cell functionality. These parameters were selected through literature review as key markers that have been found to occur with a multitude of inorganic NPs, as described in detail in Soenen *et al.*[21] For every parameter, the highest NP concentration was selected that did not lead to any negative effects, and this concentration was then further tested as the maximal "safe" concentration in the remaining assays. In the end, a substantial data set was generated for 4 nm diameter, PMA-coated Au NPs as measured under well-defined conditions and that can then be used to compare the effect of other nanomaterials that were analyzed following the same protocols. Of interest is also the final concentration of the particles that was obtained and that could be considered as a reference for labeling a variety of cells without inducing any unwanted NP-mediated side-effects.

RESULTS AND DISCUSSION

Particle Characterization. In the present work, 4 nm diameter Au NPs coated with a thick PMA layer are used (see Supporting Information for full details on NP characteristics), which are synthesized and characterized as described previously.[22] Using light-scattering and electrophoretic mobility measurements, the hydrodynamic diameter of the particles was found to be 13.9 ± 1.2 nm and the ζ-potential equaled −27.6 ± 5.6 mV in 10 mM phosphate-buffered saline (PBS) at pH 7.0. Previously, it was found by fluorescence correlation spectroscopy measurements that similar particles resulted in a hydrodynamic diameter of 12.8 ± 0.8 nm,[19] indicating the high reproducibility of particles between different synthesis batches. The particles were found to be well stable in physiological saline, as no aggregates could be noted even after 3 months of storage at ambient temperature. The Au NPs are stabilized by their negatively charged polymer shell *via* electrostatic repulsion. With regard to cytotoxic effects, similar polymer-coated Au NPs have been previously investigated.[19,23] Lehmann *et al.*[19] demonstrated increased TNFα release for polymer-coated Au NPs (below 10 nM particle concentration), but not for comparable concentrations of the polymer alone. Polymer-coated Au particles in general should be well suited for biological/biomedical applications, as they are remarkably stable. Common surfactant-coated Au NPs however have been demonstrated to partially disintegrate in solution, as surfactants such as CTAB are known to desorb from the Au surface and thereby elicit significant cytotoxic effects.[17] The PMA-coated particles that were selected as polymer-coated particles have been described to induce the lowest cytotoxic

effects, and furthermore, PMA itself was previously shown not to elicit any cytotoxic effects at concentrations up to 6.7 nM.[19] Therefore, any observed effects that would be obtained in our studies are likely to be inherent to Au NPs of similar sizes, and the particles themselves can also be considered as a good reference material. The small size of the particles is well in line with the size range commonly applied for cell-labeling purposes and is more interesting to study from both cell-labeling and toxicological points of view, as cultured cells tend to endocytose smaller sized NPs to a higher extent.

Cellular Uptake of Au NPs. Here, the Au particles were used to label C17.2 neural progenitor cells, primary HUVECs, and rat PC12 cells. All of these cells have previously been shown to be sensitive to NP-induced toxicity and further possess several interesting traits that make them well suited as basic cell types to define safe NP concentrations for labeling of a wide variety of cultured cells.[24,25] Primary HUVECs and C17.2 cells are furthermore also frequently used for transplantation studies, where the *in vitro* labeling of these cells with NPs to allow *in vivo* noninvasive monitoring of cell homing is of great importance. For these applications, it is of great importance that the NPs themselves do not interfere with the cells, to minimize any unwanted side-effects such as reduced cell migration or altered differentiation capacities that would drastically impede any progress in this field or research. The use of neural stem cell lines and primary human cells further allows determining whether any differences are observed between cell lines and primary cells, as the first display an aberrant physiology that may affect the results, whereas the latter are more closely related to actual *in vivo* conditions and may help to facilitate clinical translation of Au NP-based applications. The use of the different cell types further enhances the quality and general applicability of any data obtained, in contrast to many other studies, where NPs are tested on a single cell type that is often a cancer cell line.[17,18,26] As cancer cells have mutated in order to promote cell survival and proliferation, their contribution to nanotoxicology studies is questionable, as they are likely far more resistant to NP-mediated damage than normal cells.

When the cells were exposed to the Au NPs, a time- and concentration-dependent uptake was observed in all cell types (data not shown), where uptake levels increased almost linearly from 0, 2, 4, up to 8 h of incubation, after which a second, much slower increase in uptake was noted up to at least 24 h. As maximal cellular uptake was found after 24 h incubation, all cells were incubated with the particles for 24 h in all forthcoming experiments unless indicated otherwise. These observations are in line with previous findings by Chithrani *et al.*,[15] who found that cellular uptake of Au NPs increased in time and leveled off after 6 h of incubation. These data further show that extended incubation times up to 72 h[27] are likely not useful for enhancing cellular NP uptake. Using transmission electron microscopy (TEM), the particles were found to be located in intracellular vesicular organelles, likely endosomes (Figure 1A) for all three cell types, which is in line with literature data. The small size of the Au cores enabled visualization of the particles only at high magnification, as shown in the different TEM slices of endosomal compartments of C17.2 cells (Figure 1A1), HUVEC cells (Figure 1A2), or PC12 cells (Figure 1A3) exposed to the Au NPs at 50 nM for 24 h. The isolated location of the Au NPs and small aggregates of Au NPs within the endolysosomal compartments furthermore suggests that the PMA coating applied provides relatively good colloidal stability of the particles over a broad pH range, as unstable particles typically result in intraendosomal aggregation. This is highly important for any successful biomedical applications of these particles that typically require well-dispersed Au NPs and are severely hindered by the occurrence of high levels of aggregation.[28] Visual inspection of several cells at high magnification did not show significant amounts of NPs either in the nucleus, attached to the cell membrane, free in the cell cytoplasm, or entrapped within other organelles for cells labeled with Au NPs at 10, 20, 50, 100, or 200 nM, although these locations have been reported to eventually occur,[29] in particular with surfaces coated with certain peptides.[30] These data are in line with the general consensus that Au NPs of this size are predominantly cell-internalized through active endocytosis and the particles then remain entrapped within endosomes.

Please note that the concentration indicated in the present work refers to the number of particles per unit of volume. In the literature, NP concentrations are expressed in different units, impeding an easy comparison of results obtained. For comparative purposes, a table with the corresponding mass units can therefore be found in the Supporting Information (Supporting Table S1).

Using the results obtained by means of inductively coupled plasma (ICP)-MS measurements, the levels of cell-associated Au NPs were determined (Table 1), showing avid, concentration-dependent uptake of the PMA-coated Au NPs in all three cell types. Although intrinsic differences could be found between the different cell types, the level of cell-associated particles for all three cell types remains similar. On the basis of the TEM images and the lack of cell membrane-attached particles, it can be assumed that nearly all of these particles will be cell-internalized and located within intracellular endosomal compartments. On the basis of the total number of cells and the number of Au NPs initially applied to the cells, the cellular uptake efficiencies could be calculated (expressed as the percentage of NPs taken up with respect to the total

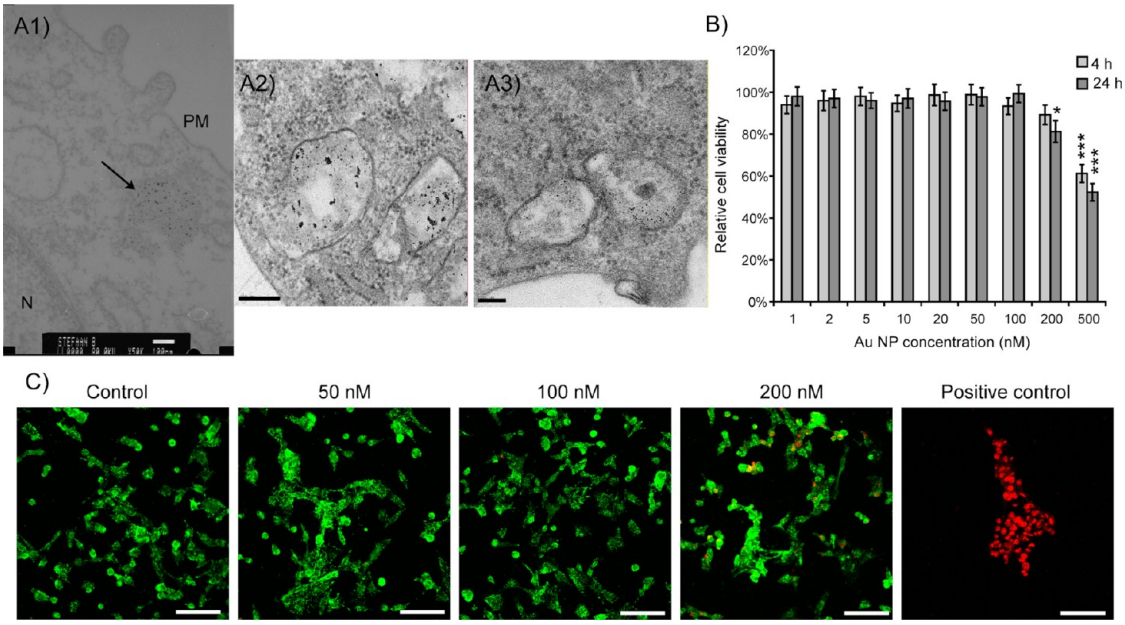

Figure 1. (A) Representative high-magnification TEM micrographs of a part of (A1) C17.2 cells, (A2) HUVEC cells, and (A3) PC12 cells incubated with Au NPs at 50 nM for 24 h showing cell-internalized particles in vesicular organelles. Scale bars: 100 nm; for A2: 200 nm. In part A1, N stands for nucleus and PM for plasma membrane. The gold particles enclosed within a vesicular structure are indicated by an arrow. (B) Relative cell viability as assessed by an LDH assay for C17.2 cells exposed to PMA-coated Au NPs at the indicated concentrations for 4 or 24 h. Data are expressed relative to that of untreated control cells (= 100%) as mean ± SEM (n = 20). The degree of significance compared to control levels is indicated when appropriate (*p < 0.05; ***p < 0.001). (C) Representative fluorescence images of calcein AM (green: live cells) and ethidium homodimer-1 (red: cells with damaged cell membrane) co-stained C17.2 cells incubated with Au NPs 0, 50, 100, or 200 nM for 24 h. The positive controls are C17.2 cells exposed to 1% Triton X-100 for 15 min prior to staining. Scale bars: 150 μm.

TABLE 1. Levels of Cell-Associated Gold Nanoparticles

	cellular NP levels (10^6 NPs/cell)		
Au NP (nM)	C17.2	HUVEC	PC12
10	0.7	0.6	0.5
20	1.3	1.1	0.9
50	2.5	2.1	1.8
100	4.5	3.8	3.1
200	7.4	6.2	5.3

number of NPs applied; more information is available in the Supporting Information). The values for all cell types were found to be decreasing for higher concentrations of the Au NPs (Supporting Table S2), indicating that cellular uptake efficiency decreases when higher concentrations of NPs are applied to the cells, which is in line with other reports.[31] On the basis of these data, the C17.2 cells were found to have the highest uptake efficiency, followed closely by HUVEC cells, whereas PC12 cells displayed the lowest cellular uptake efficiencies, possibly as a result of the small size of the PC12 cells. The high number of NPs being internalized is also within the range reported in other studies when incubation occurred in similar conditions. For example, Suggs *et al.*[32] reported that mesenchymal stem cells internalized approximately 5×10^5 Au NPs/cell for 20 nm diameter citrate-coated Au NPs. The slightly higher values reported in our study are likely due to the smaller size of the particles and intrinsic differences in the uptake capacities of the cell types used.

Effects of Au NPs on Cell Viability. Cells were then exposed to a broad concentration range of Au NPs (1−500 nM) for 2, 4, 8, 12, or 24 h. The concentrations selected here correspond to the range of concentrations frequently applied in biomedical applications of Au NPs, as can be supported by literature data in the field, where, for instance, 200 μg/mL or 400 nM (100 μg/mL) was used for *in vitro* cancer therapy studies or 151 μg/mL for *in vivo* biodistribution studies.[28,33,34] In terms of acute cytotoxicity, a concentration- and time-dependent effect of the particles could be observed, where maximal effects were found after 24 h incubation at the highest NP concentration. Figure 1B shows the data after 4 and 24 h for C17.2 cells, showing a slight but significant decrease in cell viability assessed by a lactate dehydrogenase (LDH) assay at 24 h incubation at 200 nM and a large diminution of cell viability when cells were exposed to 500 nM Au NPs. Similar effects were observed for the HUVECs and PC12 cells, where no acute cytotoxicity could be noted at 100 nM Au NPs for any of the cell types (see Supporting Figure S1). Also, when cells were exposed to medium preincubated with the Au NPs for 24 h after which the Au NPs were removed by ultracentrifugation, no effect on cell viability could be seen (Supporting Figure S2), indicating that the decrease in cell viability was caused by immediate exposure of the cells to the NPs and not

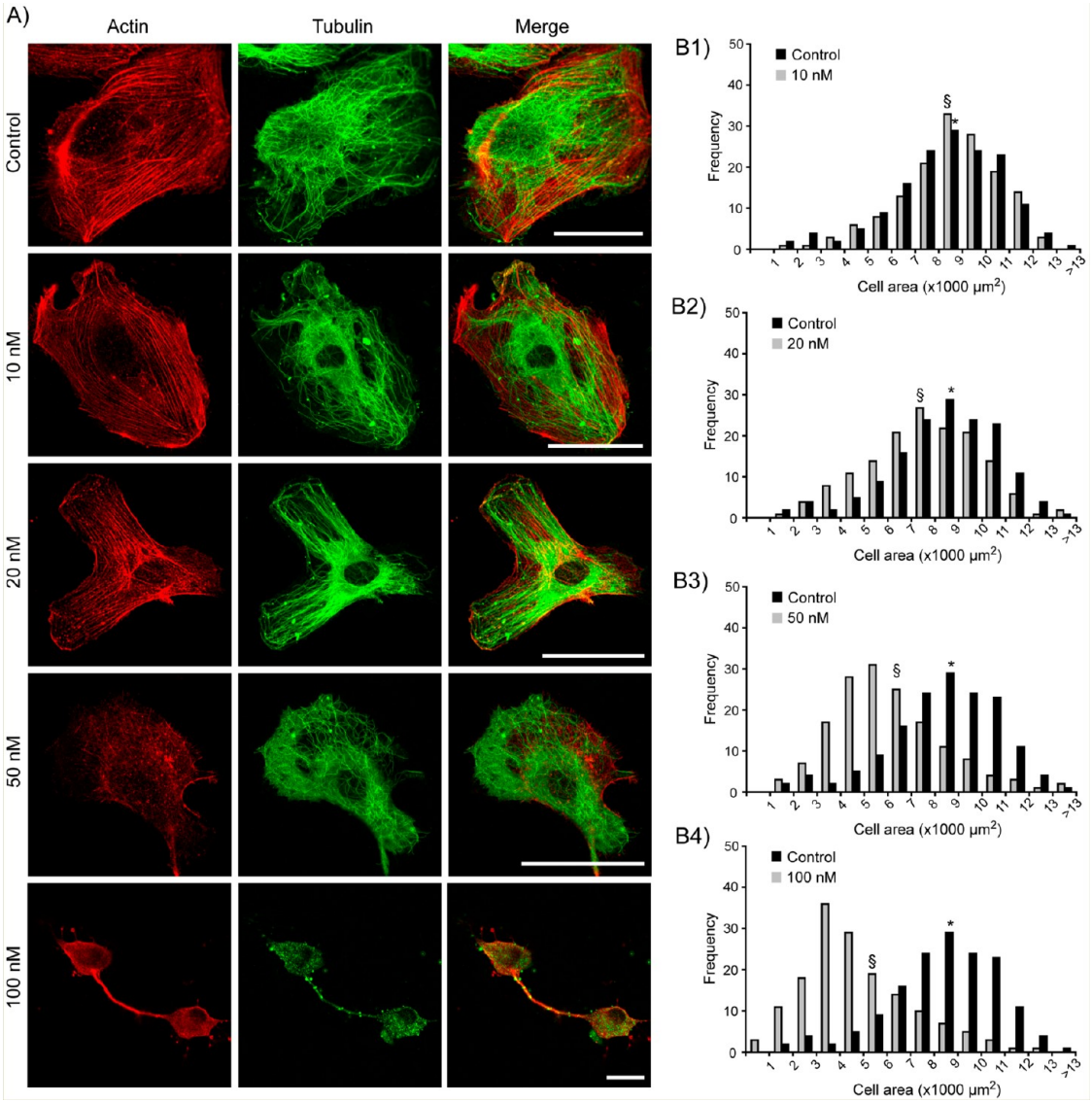

Figure 2. (A) Representative confocal images of control HUVECs or cells exposed to 10, 20, 50, or 100 nM Au NP for 24 h at 1 day post-NP-labeling. The left column depicts actin staining (red), the middle column depicts α-tubulin (green), and the right column is a merged image of both actin and α-tubulin. Scale bars: 50 μm. (B) Histograms representing the cell areas of control cells (dark gray) and cells incubated for 24 h with Au NPs at 10 nM (B1), 20 nM (B2), 50 nM (B3), and 100 nM (B4). The average cell area is indicated with (*) for control cells and with (§) for NP-treated cells.

by secondary effects such as binding and clearance of nutrients by the NPs. These obtained results are in the expected range, as similar PMA-coated 4 nm diameter Au NPs were found not to induce any acute cytotoxic effects on malignant T lymphocytes for concentrations tested up to 50 nM Au NPs.[23]

Cellular co-staining with calcein AM (green: viable cells) and ethidium homodimer-1 (red nucleus: cells with damaged plasma membrane) confirmed the lack of cytotoxic effects at 50 and 100 nM Au NPs, whereas 200 nM Au NPs resulted in the onset of cytotoxic effects (Figure 1C). As NPs are known to be able to interfere with common viability assays, the confirmation of the results obtained by the LDH further supports that the effects that were observed are authentic and not caused by undesired side-reactions.

Effects of Au NPs on Cell Cytoskeleton and Cell Spreading. As the main goal of the present work is to evaluate cellular stress at the highest, nontoxic concentrations of Au NPs, the maximal concentration that was further used in this work was 100 nM. One possible sign of cellular stress induced by uptake of nanosized materials is alterations to the cytoskeleton network.[21] Therefore, the effect of the PMA-coated Au NPs on cellular actin and tubulin fibers was investigated. To this end, control cells and cells incubated with Au NPs at 10, 20, 50, or 100 nM for 24 h were stained for F-actin (red) and α-tubulin (green) at 1 day post-NP-incubation. The results shown in Figure 2 are for HUVEC cells, as these cells are typically well-spread and display an extensive actin and tubulin network, which facilitates the analysis of any defects. Figure 2A shows representative confocal

images of the different channels as well as an overlay image of both the actin and tubulin cytoskeleton. Figure 2B displays histograms of cell areas of control cells or cells incubated with the Au NPs at 10, 20, 50, or 100 nM. On the basis of the images, no effects were observable for cells exposed to 10 or 20 nM Au NPs, but a clear loss of actin network coherence can be observed when cells were exposed to Au NPs at 50 nM. Similarly, a clear loss of tubulin network can also be observed at Au NP concentrations of 100 nM. These profound effects on cytoskeleton architecture also resulted in a concentration-dependent reduction of cell spreading (Figure 2B). Similar results were obtained for C17.2 neural progenitor cells (Supporting Figure S3), where the overall trend was similar in that higher NP levels (50 nM or above) reduced cell spreading, but the smaller size of C17.2 cells together with the occurrence of cytoplasmic extensions typical for cells of neural lineage results in a reduced extent of these effects. PC12 cells could not be analyzed in this assay due to the small size of the cells and very limited cytoplasmic space as well as the semiadherent nature of the cells that only display minimal cell spreading. Of further interest is the fact that these effects were found to be transient, where the degree of spreading of cells exposed to particles at 100 nM gradually reaches the level of control cells in approximately 6−8 days (Supporting Figure S4). Although the average cell physiology recovers in time, the fate of the cells with initial aberrant physiology remains unclear. It is well possible that cells with lower NP numbers and less NP-induced stress will show a favorable cell division rate, which will lead to a rapid increase in the number of healthy cells with normal physiology but containing only minimal amounts of particles, possibly too low for any biomedical application. Alternatively, the cells that show the highest amount of stress could eventually die at a later stage, resulting in only healthy cells (with low particle numbers), which are able to proliferate. The latter hypothesis seems less likely, as additional LDH assays at later time points did not reveal any signs of cell death within one week after NP exposure at 100 nM (Supporting Figure S5), but the gradual loss of low numbers of cells below the sensitivity threshold of the assay cannot be excluded. Furthermore, when cells were exposed to medium that was preincubated with the Au NPs at 10, 20, 50, or 100 nM for 24 h, after which the NPs were removed by centrifugation, no effects on cell morphology could be observed (data not shown), suggesting that the morphological aberrations are directly caused by the Au NPs and are not due to the loss of nutrients or growth factors that are bound to the NP surfaces.

Together, the data show a transient and concentration-dependent deregulation of both the actin and tubulin cytoskeleton architectures. It is worth noting that effects on the actin cytoskeleton occurred at levels (50 nM) lower than those at which the tubulin network was deformed (100 nM), suggesting that the actin fibers are—for reasons that are presently unclear—more sensitive to the NP-induced deformations. Although Au NP-mediated cytoskeletal aberrations have not been carefully studied thus far, several authors have reported on morphological defects of, for instance, A549 human lung carcinoma cells[11] or human dermal fibroblasts[35] as a consequence of Au NPs. In line with our present findings, Au NP concentration-dependent perturbations of actin fibrils have been described.[35,36] Interestingly, Au NP-induced cytoskeletal deformations have thus been described to occur in multiple cell types and have been induced with a variety of Au NPs varying in size from 4 to 45 nm and with different coating agents (PMA, citric acid). As such, it appears that the deformation of cytoskeletal architecture is a common, concentration-dependent mechanism of Au NPs and therefore an important parameter to consider when determining the toxicological profile of Au NPs.[21]

The underlying mechanism for these cytoskeletal defects are as of yet unclear, but the lack of any particles found freely in the cytoplasm together with previous data by Mironava *et al.*,[36] who observed actin deformations while actin protein expression levels were unaffected, suggests an indirect mechanism to be at play. We hypothesize that high intracellular numbers of nondegradable and solid NPs that are clustered together in large endosomal structures, typically located in the perinuclear region,[11] may sterically hinder and deform the cytoskeletal architecture. It has been described that NP-loaded endolysosomal structures enlarge in size and lose their functionality. As these endolysosomal vesicles are typically located in the perinuclear region and near the microtubule organizing center, we suggest that they may sterically hinder the existing or newly forming cytoskeletal structures, along with interfering with cell division. This hypothesis is further supported in previous studies where similar morphological defects were observed for iron oxide NPs,[25,37,38] suggesting a common effect for solid, endosomally located NPs. Further studies on this phenomenon are required to unravel the precise underlying mechanisms.

Effects of Au NPs on focal adhesions and associated signaling. The previous work on iron oxide NPs further showed that extensive deformation of the actin fibers may have secondary effects on actin-mediated signaling pathways.[38] To investigate this possibility, the effect of the Au NPs on focal adhesion complexes (FACs) was studied. Figure 3A shows representative confocal images of control HUVEC cells or cells incubated with the PMA-coated Au NPs for 24 h at 10, 20, 50, or 100 nM. The images displayed reveal the actin cytoskeleton (red) and vinculin protein (green), an important structural component of FACs present in nearly all cell

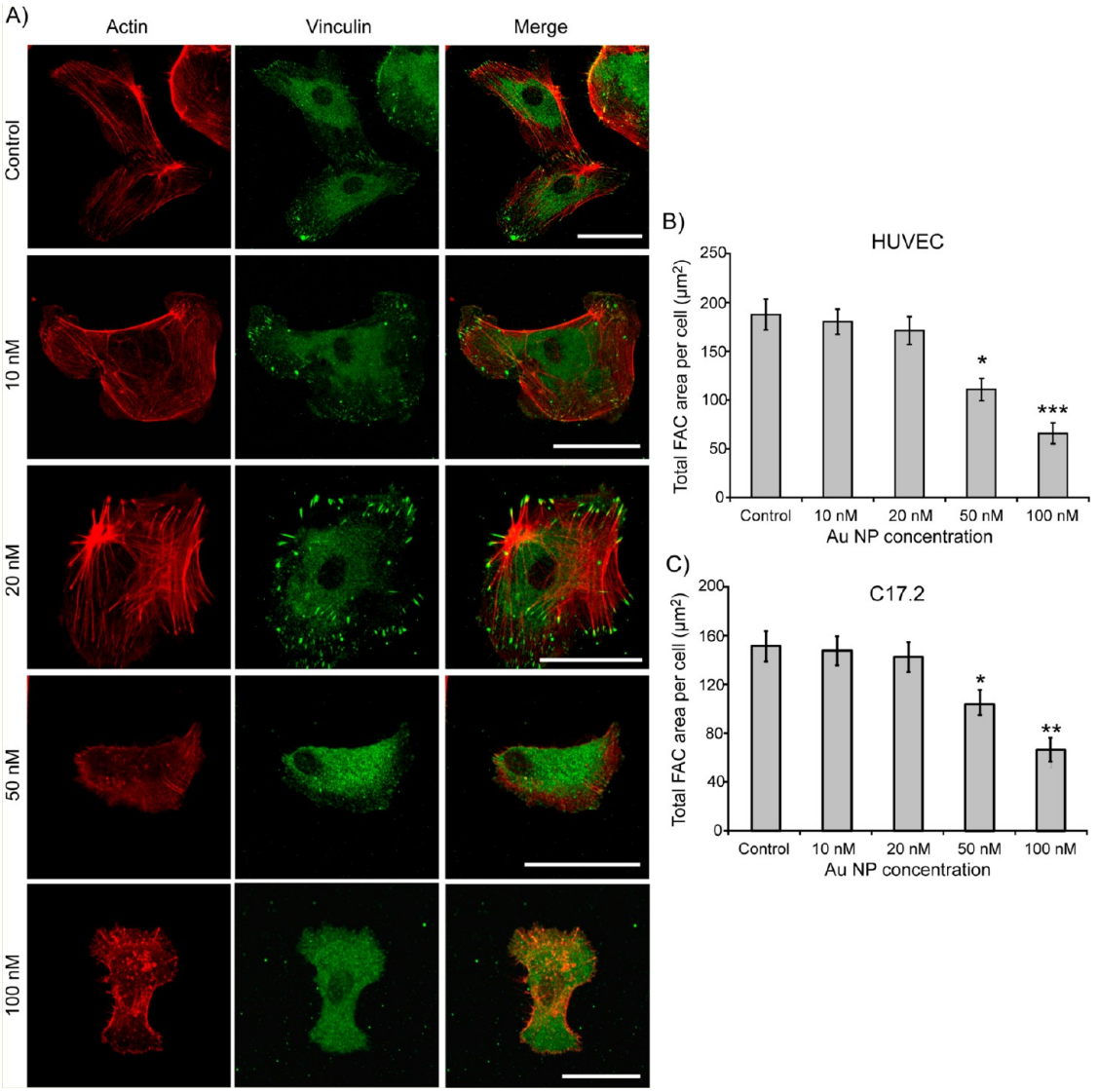

Figure 3. (A) Representative confocal images of control HUVECs or cells exposed to 10, 20, 50, or 100 nM Au NP for 24 h at 1 day post-NP-labeling. The left column depicts actin staining (red), the middle column depicts vinculin (green), and the right column is a merged image of both actin and vinculin. Scale bars: 50 μm. (B, C) Histogram representing the cellular FAC areas of control cells or cells incubated with the Au NPs for 24 h at 10, 20, 50, or 100 nM for (B) HUVEC cells and (C) C17.2 cells. Data are expressed as mean $\pm$ SEM ($n = 20$). When appropriate the degree of significance is indicated for Au NP-treated cells compared with untreated control cells (*$p < 0.05$; **$p < 0.01$; ***$p < 0.001$).

types.[39] Similar to the data shown in Figure 2, the control cells show clear actin fibers, whereas Au NP-treated cells display an extensive loss of actin fibers, at both 50 and 100 nM incubation. Similarly, control cells show nicely mature FACs, as can be seen by the highly intense vinculin stainings localized preferably where several actin fibers end. For cells exposed to the Au NPs at either 50 or 100 nM, the loss of the actin network correlates with a decrease in FACs and an apparent increase in the amount of free vinculin, which is typically seen as a diffuse staining throughout the cellular cytoplasm. By analyzing the images, the total area of the FACs per cell in every condition could be calculated (Figure 3B), showing a significant decrease in cellular FAC area for cells exposed to the PMA-coated Au NPs at 50 nM and an even bigger reduction of FAC areas for cells exposed to 100 nM Au NPs. C17.2 cells displayed overall smaller FAC areas due to their smaller size, but resulted in similar effects on FAC area reductions when cells were exposed to higher levels of Au NPs (Figure 3C).

As the FAC areas are the product of the number of FACs and their respective size (which correlates to their maturity), the large reduction in FAC areas indicates a significant loss of mature FACs. FACs are multiprotein complexes that form a direct link between the actin network and the extracellular environment and thereby play an important role in actin-mediated signaling (*e.g.*, integrin-triggered signaling).[40] The Au NP-mediated loss of mature FACs therefore implies significant alterations in intracellular signaling pathways, which could manifest itself in a large variety of defects

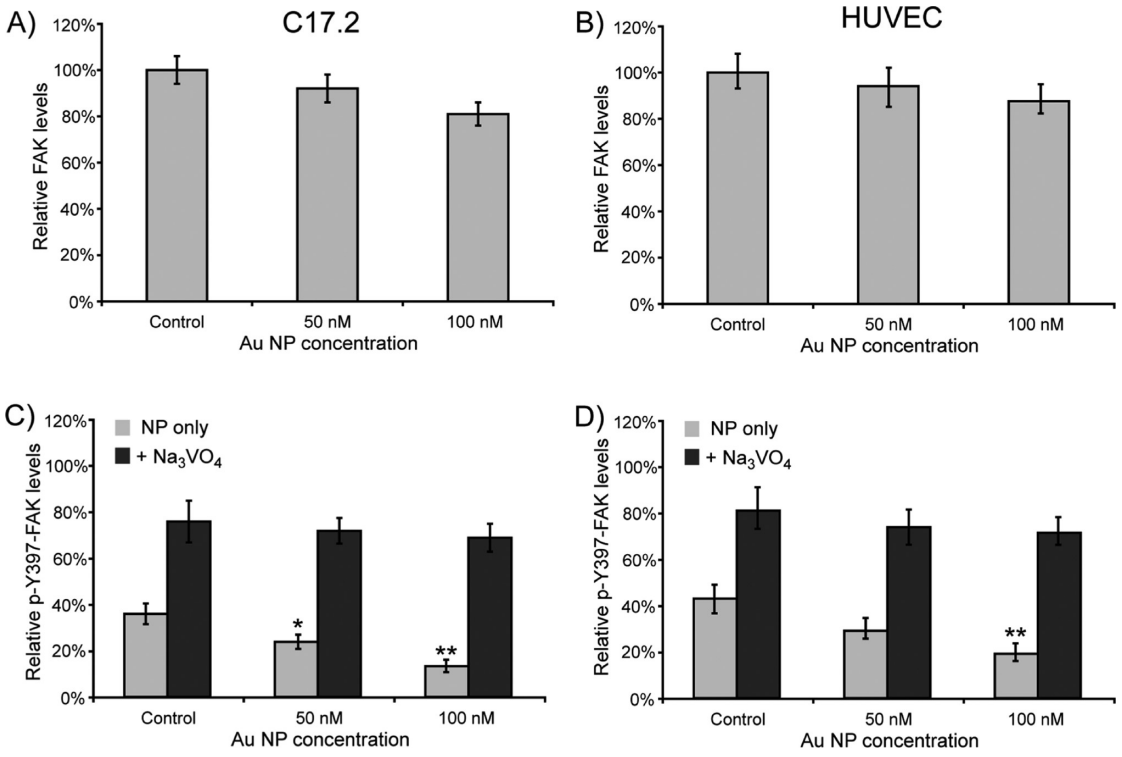

Figure 4. Level of FAK expression of 5×10^4 cells expressed as (A, B) the amount of total cellular FAK or (C, D) the amount of active pY397-FAK relative to control cells (100%) after 2 days following exposure of the cells to Au NPs at 50 or 100 nM for 24 h. The levels of FAK in C17.2 cells are shown in (A) and (C); for HUVEC cells in (B) and (D). The dark gray bars indicate cells that were additionally exposed to 100 μM Na_3VO_4 for 5 h immediately prior to protein extraction and are expressed as the total amount of pY397-FAK relative to the respective total expression level of FAK for every condition. The data are presented as the mean $\pm$ SEM ($n = 3$ independent assays). When appropriate the degree of significance is indicated for Au NP-treated cells compared with untreated control cells (*$p < 0.05$; **$p < 0.01$).

in cell homeostasis and should thus be considered as a highly unwanted and extremely dangerous toxicological effect of the Au NPs on the labeled cells.

In order to further investigate the potential consequences of the observed effects on actin-mediated signaling mechanisms, we determined the protein expression levels of focal adhesion kinase (FAK), one of the main signaling molecules involved in a variety of actin-mediated signaling pathways. FAK is a nonreceptor protein-tyrosine kinase that predominantly localizes in FACs. Upon integrin stimulation, FAK can autophosphorylate at Y397, after which it can bind Src family member kinases, which can further phosphorylate FAK and act synergistically to phosphorylate downstream targets.[39] Figure 4 shows the total levels of FAK protein in (A) C17.2 or (B) HUVEC cells for either control cells or cells incubated with PMA-coated Au NPs at 50 or 100 nM for 24 h. The data clearly show a small, but nonsignificant concentration-dependent decrease of FAK levels, indicating no clear effects of the Au NPs on protein expression levels. As only Y397-phosphorylated (pY397) FAK is involved in actin-mediated signaling, the level of pY397-FAK was evaluated as well (Figure 4C,D), clearly showing a significant and concentration-dependent decrease of active pY397-FAK levels upon exposure of either (C) C17.2 or (D) HUVEC cells to the Au NPs. Pretreatment of the cells for 5 h with 100 μM sodium orthovanadate, an inhibitor of protein phosphotyrosyl phosphatases, was able to increase the level of pY397-FAK to approximately 75% of their respective total expression levels for both control and Au NP-treated cells.

The lack of any effects on FAK expression levels, but the severe decrease of FAK activation further supports our previous hypothesis that the observed effects are due to secondary (indirect) effects of the Au NPs, likely due to steric hindrance and physical deformation of the actin network by large endosomal compartments containing high concentrations of Au NPs. The actin network remodeling will break up the FACs, thereby drastically impeding any activation of FAK that is functionally linked to mature and stable FACs.[39] This then results in a sort of snowball effect, as the lower levels of active FAK will lead to less activation of paxillin, an important signaling molecule involved in the growth of actin fibers.[39] The reduced actin remodeling capabilities are thus likely to further enlarge the initial cytoskeletal aberrations induced directly by the Au NPs, resulting in the distinct effects as seen in Figure 2.

Effects of Au NP-Induced Cytoskeletal Deformations on Cell Homeostasis. *Effects of Au NPs on Cell Proliferation.* The

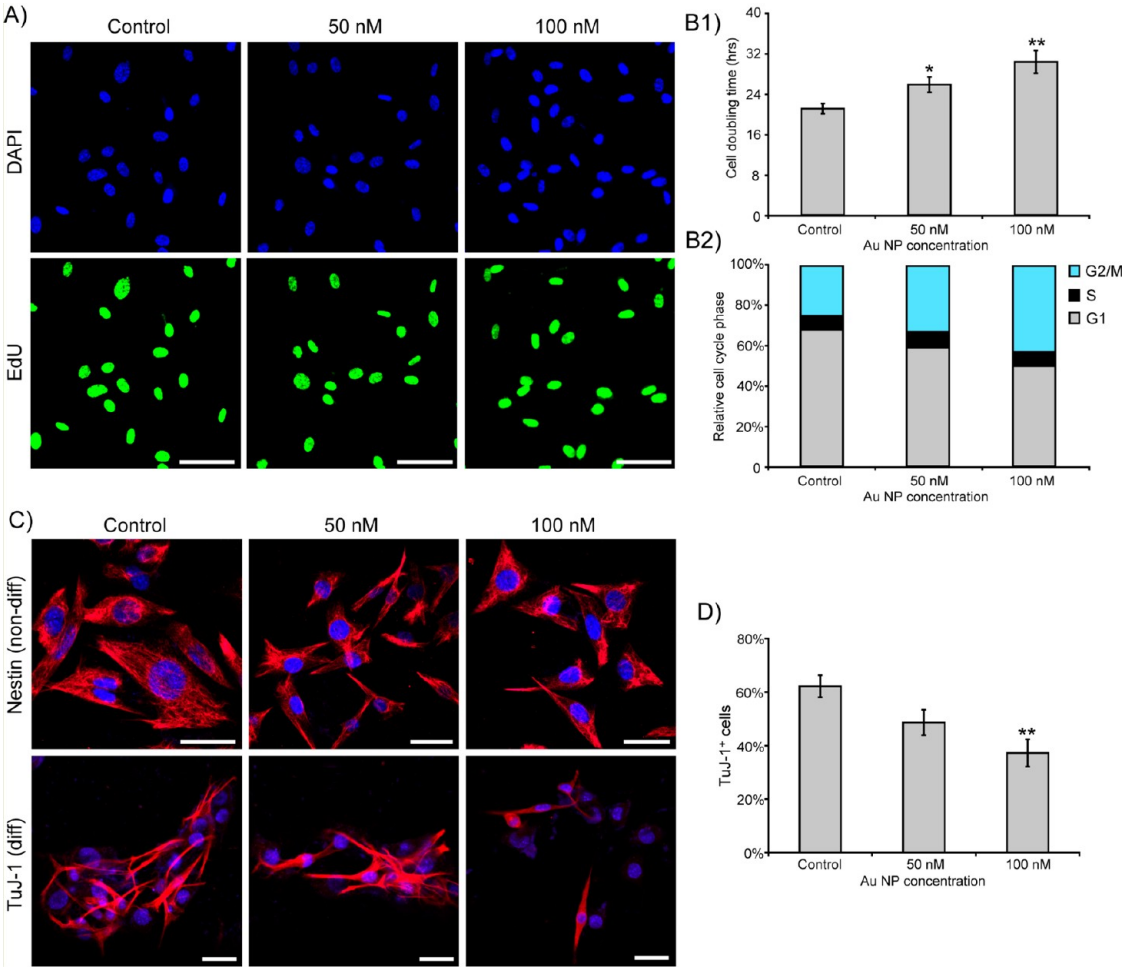

Figure 5. (A) Representative fluorescence images of C17.2 cells incubated with Au NPs at 0, 50, or 100 nM for 24 h, kept in culture for another 24 h, and subsequently incubated with EdU for 12 h to indicate cellular proliferation. All nuclei are counterstained by DAPI (blue); the nuclei of cells going through the S phase of mitosis have incorporated EdU (green). Scale bars: 100 μm. (B1) Cell doubling times of C17.2 cells for control cells or cells incubated with Au NPs for 24 h assessed at 3 days after NP incubation. Data are expressed as mean $\pm$ SEM (n = 5). When appropriate, the degree of significance compared to untreated control cells is indicated (*p < 0.05; **p < 0.01). (B2) The respective cell cycle statuses of control cells or cells incubated with Au NPs for 24 h assessed at 2 days after NP incubation by flow cytometry. The relative amount of cells in G1 phase is indicated in gray, S phase in black, and G2/M phases in light blue. (C) Representative confocal images of C17.2 cells incubated with Au NPs for 24 h, showing DAPI nuclear counterstain in all cells (blue) and those stained for the presence of nestin in proliferating cells (top row) or for TuJ-1 for cells undergoing 6 days of neuronal differentiation (bottom row). Scale bars: 50 μm. (D) Number of TuJ-1 expressing cells relative to the total number of cells. Data are expressed as mean $\pm$ SEM (n = 3). The degree of significance between Au NP-exposed cells and control cells is given when appropriate (p < 0.01).**

lower levels of active pY397-FAK can have a wide range of effects on the cellular well-being due to the high number of intracellular signaling pathways that are linked to FAK-mediated signaling. In order to evaluate whether the reduced pY397-FAK levels lead to any secondary effects, cell proliferation was analyzed, as cell cycle progression is known to be one of the major downstream effectors of FAK-mediated signaling.[41] Figure 5A shows representative fluorescence images of C17.2 control cells or cells incubated with the Au NPs for 24 h at 50 or 100 nM. All cell nuclei are stained with DAPI (blue) regardless of their cell cycle phase, whereas cells were also exposed to 5-ethynyl-2′-deoxyuridine (EdU; green), a thymidine analogue that can be incorporated in the cellular nuclear DNA upon DNA synthesis (S phase of cell cycle). From the images, it can be seen that cells exposed to the Au NPs at 100 nM did not all progress through the S phase of the cell cycle, in contrast to control cells or cells treated with 50 nM Au NPs. As no toxic effects were found at the concentrations used (Figure 1), this likely points to a halt in cell cycle progression, possibly due to altered signaling mechanisms. By means of manual cell counting, it was further shown that the exposure of C17.2 cells to the Au NPs led to a significant and concentration-dependent reduction in cell cycle progression (Figure 5B1). Similar effects were observed for the HUVEC cells, showing a significant, concentration-dependent reduction of cell division (Supporting Figure S6). To investigate this more thoroughly, the exact cell cycle phase of control and treated samples was analyzed (Figure 5B2). The data show that the percentage of C17.2 cells in the

S phase did not alter much among the different samples (±8% of all cells). However, for cells exposed to the Au NPs, a concentration-dependent increase of cells in the G2/M phase of the cell cycle could be seen correlated with a decrease of cells in G1 phase.

These data point to an arrest of the cells in G2/M phase upon exposure to the Au NPs at 50 or 100 nM. This can be explained by the low activation status of FAK, which has been shown to inhibit proliferation.[41] When FAK is activated, downstream signaling events trigger the expression of S-phase-associated kinase protein 2 (Skp2), an F-box protein that targets inhibitors of cyclin-dependent kinases (CDKs), such as p21 and p27.[42] The lower levels of active FAK will thus generate less Skp2 expression, which in turn will lead to more p27-mediated inhibition of cyclin E/CDK2 complex formation, thereby impeding G2/M phase transition.

Effects of Au NPs on Stem Cell Differentiation. Other than affecting cell proliferation kinetics, one of the major concerns of nanosized material on cultured stem cells is possible alterations of the cellular "stemness", *i.e.*, the ability to self-renew by undergoing mitosis and the ability to differentiate into more mature cell types. To look at any effects of the Au NP-mediated altered intracellular signaling on cell differentiation capabilities, the expression of cellular markers in C17.2 cells undergoing neural differentiation has been evaluated. C17.2 cells are an immortalized neural progenitor cell line obtained by transduction of neural progenitor cells derived from the external germinal layer of neonatal mouse cerebellum with the immortalizing oncogene v-myc.[43] The ability of these progenitor cells to further differentiate into mature neurons has been tested for both control cells and cells exposed to the Au NPs for 24 h at 50 or 100 nM. Figure 5C shows that in all conditions proliferating cells express nestin, a type VI intermediate filament that is a typical marker for neural stem cells, whereas no cells revealed any expression of α-tubulin III (TuJ-1), a neuron-specific α-tubulin isoform (data not shown). Upon 7 days of neuronal differentiation, control cells showed high expression of TuJ-1, indicative of successful differentiation of the C17.2 cells from a progenitor state into a mature neuron. Cells that were incubated with the Au NPs at 50 nM also showed high TuJ-1 expression levels, although the number of cells that were successfully differentiated was slightly less than for the control cells (Figure 5D). Cells that were exposed to 100 nM Au NPs displayed drastically reduced TuJ-1 expression levels, resulting in a significant inhibition of stem cell differentiation capacities due to the Au NP-mediated cellular effects. Please note that these effects are well in line with the observed effects on the cytoskeleton deformations. Although the effects on the cytoskeleton architecture are only transient and most cells appear "normal" after 7 days of continuous culture (Figure 5C, top row), the secondary effects caused by these deformations are still present. Therefore, when investigating cell−NP interactions, it is imperative to study a multitude of parameters and to also avoid any transient effects if particles are to be used for biological purposes.

The effects of Au NPs on cell functionality have not been studied in depth, but several articles have already indicated the possible dangers of Au NPs on impeding cellular functions. Pernodet *et al.*[35] noted that very high concentrations of citrate-coated Au NPs decreased the migration capacity of human dermal fibroblasts. On the level of stem cell differentiation, a lot of ambiguity still remains, as contradicting results can be found. Li *et al.*[44,45] observed that 15 and 30 nm diameter Au NPs slightly inhibited both osteogenic and adipogenic differentiation of human mesenchymal stem cells, whereas Zhang *et al.*[46] reported that Au NPs stimulated osteogenesis and impeded adipogenesis of mesenchymal stem cells. These data clearly support our present findings and indicate that the intracellular presence of Au NPs can have broad effects on a variety of signaling mechanisms. As cellular morphology has large influences on stem cell differentiation,[47] we suggest that the sterically induced deformations of the actin network by the Au NPs are likely a key player in contributing to this unwanted and dangerous effect.

Induction of Reactive Oxygen Species. Next, we investigated whether additional mechanisms other than cell cytoskeleton deformations played a role in the cytotoxic effects elicited by the Au NPs. André Nel and coworkers have previously described that a broad range of nanomaterials are known to induce ROS, and they put forward ROS induction as one of the main damaging effects of NPs on cell physiology.[48,49] For Au NPs, the induction of ROS has also been described in several studies,[27] hereby making it a likely candidate for the observed decrease in cell viability at higher concentration of Au NPs. To verify this, cells were exposed to PMA-coated Au NPs for 24 h at concentrations ranging from 1 to 200 nM. As shown for C17.2 cells in Figure 6A, a clear concentration-dependent induction of ROS was observed, reaching significantly elevated levels at 50 nM Au NPs and resulting in a 2.5-fold increase of 200 nM Au NP-treated cells compared to control cells. Similar results were obtained for the HUVEC and PC12 cells (Supporting Figure S7), where the level of ROS in PC12 cells is only slightly lower than in the case of C17.2 cells. Taking into account the lower cellular uptake of the PC12 cells, this suggests that the PC12 cells are more sensitive to NP-induced stress than the C17.2 or HUVEC cells. At shorter incubation times, only minimal ROS elevations were observed (data not shown), likely due to the lower intracellular amount of particles, and the time required for cells to react to the presence of the foreign material by generating ROS

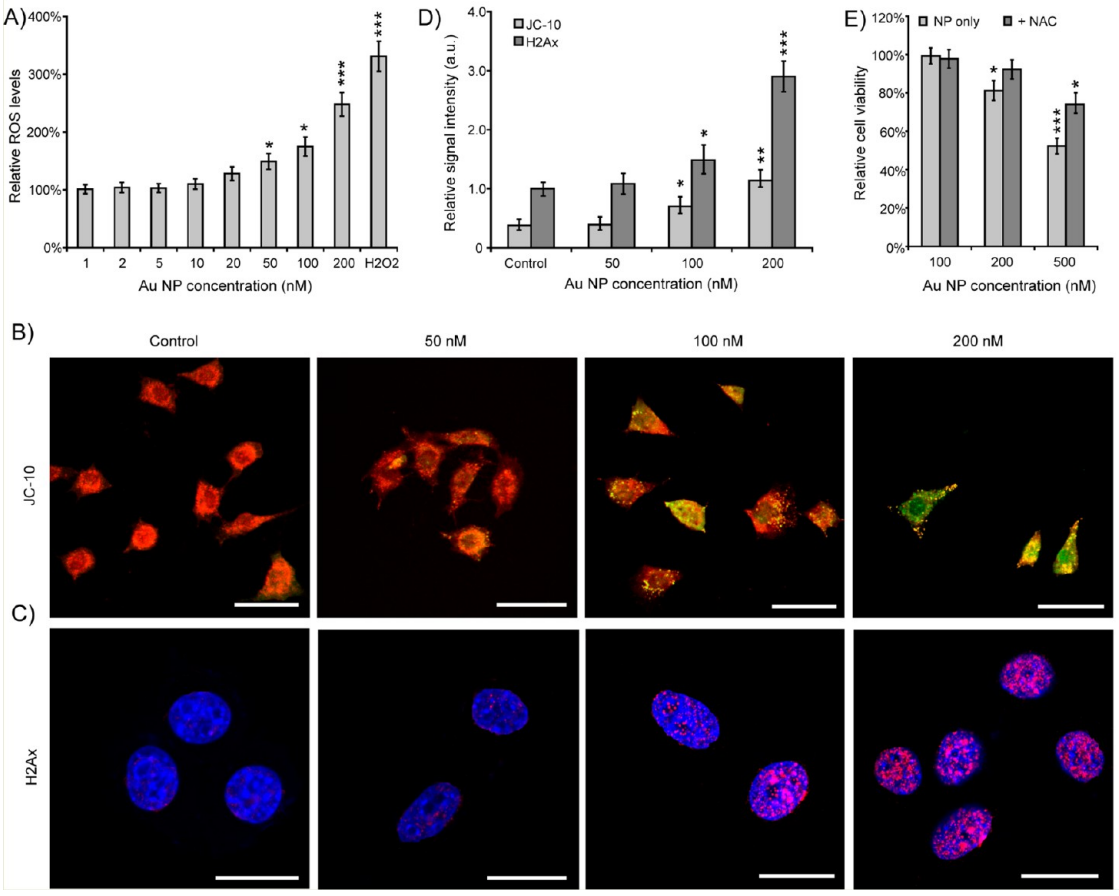

Figure 6. (A) Relative levels of ROS in C17.2 cells incubated for 24 h with Au NPs at the concentrations indicated as determined by CM-H_2DCFDA. As a positive control, cells were exposed to 1% H_2O_2 for 2 h. Values are expressed relative to untreated control cells (= 100%) as mean ± SEM (n = 5). (B, C) Representative confocal images of C17.2 cells incubated with Au NPs for 24 h at 0, 50, 100, or 200 nM. (B) Cells were stained for mitochondrial membrane potential using JC-10 (red: healthy mitochondria; green: damaged mitochondria). (C) Cells were stained for DNA double strand break marker γ-H_2Ax (red) and counterstained using DAPI nuclear counterstain (blue). Scale bars: (B) 75 μm; (C) 20 μm. (D) Quantitative levels of JC-10 (light gray) or γ-H_2Ax (dark gray) expressed as the ratio of green over red fluorescence for JC-10 and fluorescence intensity levels relative to those of untreated controls (= 1) for γ-H_2Ax. Data are expressed as mean ± SEM (n = 3). (E) Relative cell viability as assessed by an LDH assay for C17.2 cells exposed to Au NPs at 50, 100, or 200 nM for 24 h in the absence (light gray) or presence of 5 mM NAC (dark gray). Data are expressed relative to that of untreated control cells (= 100%) as mean ± SEM (n = 20). (A, D, E) When appropriate, the degree of significance is indicated (*p < 0.05; **p < 0.01; ***p < 0.001).

as 24 h is commonly found as the optimal time to assess ROS levels upon NP exposure.[50] The induction of ROS can help the cells in overcoming stress induced by ingesting foreign materials and is thus a logical response for cells incubated with solid inorganic NPs. In order to protect the host cells from the possible dangers of ROS, mammalian cells possess several protective agents, such as superoxide dismutase or glutathione, that aid in the transformation of ROS species into less reactive substances. Because of the cellular defensive capabilities against ROS, the consequences of an elevated ROS level on cell physiology is unclear and differs widely among various cell types.[51] Highly elevated ROS levels may potentially initiate lipid peroxidation and protein oxidation, induce DNA damage, or affect mitochondrial viability, which can then lead to cell death.

Secondary ROS-Mediated Effects. To evaluate whether the elevated ROS levels have any secondary effects on cell physiology, mitochondrial membrane potential ($\Delta\Psi_m$) and DNA damage were evaluated. Figure 6B shows representative fluorescence images of C17.2 cells exposed to Au NPs at 0, 50, 100, or 200 nM for 24 h and subsequently stained for $\Delta\Psi_m$ using the JC-10 dye. This is a cationic carbocyanine compound that can bind the outer mitochondrial membrane, and in healthy mitochondria with a normal $\Delta\Psi_m$, the dye will aggregate inside the mitochondria (red color), whereas the dye will remain as green monomers throughout the cell cytoplasm in the case where the $\Delta\Psi_m$ has been lost. Using this approach, mitochondrial damage will result in an increased ratio of green over red fluorescence. The images show control cells with distinct red-colored mitochondria, which is similar for cells exposed to 50 nM Au NPs. The ratio of green over red fluorescence was also measured spectrofluorometrically (Figure 6D), where it can be seen that for cells exposed to the particles at 100 nM a clear increase in green

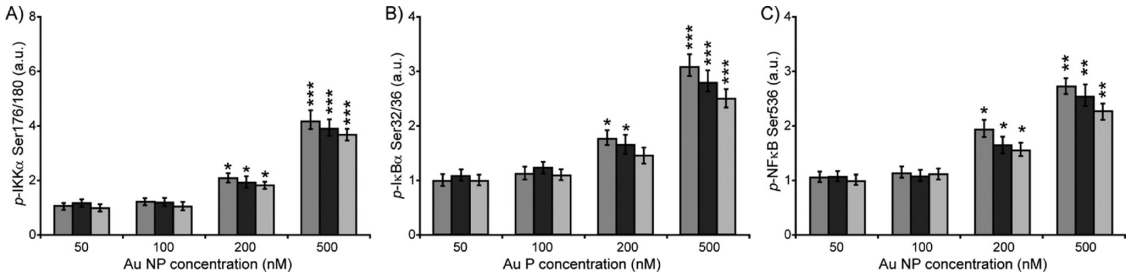

Figure 7. Activation of the NFκB pathway by Au NPs. C17.2 (gray), HUVEC (dark gray), and PC12 cells (light gray) were incubated with 50, 100, 200, or 500 nM Au NPs for 24 h, after which the levels of (A) activated IKKα, (B) activated IκBα, and (C) activated NFκB were determined using an ELISA assay. Data are expressed as mean ± SEM (n = 3).

fluorescence and a decrease in red fluorescence can be seen, which is even more pronounced for cells exposed to 200 nM Au NPs. For HUVEC and PC12 cells, similar results were obtained where mitochondrial damage was noticeable at concentrations of 100 nM and above (Supporting Figure S8).

In terms of possible DNA damage, the occurrence of double-strand breaks was evaluated by staining for γ-H_2Ax foci, which are formed by the rapid phosphorylation of histone H_2Ax at sites of DNA double-strand breaks.[52] Figure 6C shows representative confocal images of C17.2 cells stained for γ-H_2Ax and where the nuclei have been counterstained using DAPI. On the basis of these images, it is clear that the cells display a concentration-dependent increase in γ-H_2Ax foci correlated with higher NP levels. By analyzing the fluorescence levels of the images (Figure 6D), it is further shown that 100 nM Au NPs lead to slight but insignificant increases in γ-H_2Ax foci, but when cells are exposed to 200 nM Au NPs, a significant 3-fold increase in the overall fluorescence level is observed, indicating high levels of DNA double-strand breaks. For HUVEC and PC12 cells, significant levels of γ-H_2Ax were obtained for HUVEC cells exposed to Au NPs at 100 nM or above, where effects on HUVEC cells were most pronounced (Supporting Figure S8), possibly indicating a higher sensitivity of primary HUVEC cells to oxidative DNA damage than long-lived cell lines such as C17.2 or PC12 cells.

Taken together, these data point to severe secondary effects of the elevated ROS levels when cells were exposed to Au NPs at concentrations of 200 nM. As these results are in line with the onset of cytotoxic effects, the link between ROS induction and the decrease in cell viability was further looked into. An important mediator in ROS-induced cell death-mediated signaling is nuclear factor kappa B (NFκB). NFκB has been described to be activated upon oxidative stress induced by nanomaterials such as quantum dots.[53] Upon ROS induction, IkappaB kinases (IKK) phosphorylate and trigger degradation of inhibitory IκB proteins. This enables the release of bound NFκB dimers, resulting in a translocation from the cell cytoplasm into the nucleus, where the NFκB dimers can act as transcription factors.

When cells were exposed to 50, 100, 200, or 500 nM Au NPs for 24 h, activation of the NFκB pathway was observed at the highest concentrations, reaching significant levels at 200 nM Au NPs, which is in line with the occurrence of cytotoxicity at these concentrations (Figure 7A–C). The clear correlation of NFκB activation with ROS levels suggests that NFκB activation results from oxidative stress. Given that the effects for the three cell types are comparable, this further highlights the sensitivity of the PC12 cells toward nanomaterial-induced oxidative stress.

In order to link the ROS levels to the cytotoxic effects observed, cells were co-incubated with Au NPs and 5 mM *N*-acetylcysteine (NAC), an FDA-approved ROS scavenger. Exposure of the cells to the Au NPs in the presence of 5 mM NAC significantly reduced ROS levels in all three cell types, back to near control levels (Supporting Figure S9). Under these low ROS conditions, both mitochondrial and DNA damage were found to be abolished and no activation of NFκB was found (Supporting Figures S10, S11). Furthermore, cell viability could be partially recovered in all three cell types (Figure 6E, Supporting Figure S12). Interestingly, however, is the fact that treatment of the cells with NAC was not sufficient to overcome all the cytotoxic effects of the Au NPs at the highest concentration, especially in the case of C17.2 and HUVEC cells. This suggests the role of additional ROS-independent mechanisms taking place that are more pronounced for the C17.2 and HUVEC cells. One possibility is the cytoskeleton deformations that are contributing to the cytotoxic profile of the particles. This was further confirmed by the lack of effect of 5 mM NAC on FAK activation levels (Supporting Figure S13), confirming that the observed cytoskeletal rearrangements and altered signaling pathways occurred in a ROS-independent manner and affect cell viability through an independent mechanism.

Effects of Au NPs on Cell Functionality. For biomedical applications, stem or immune cells are often cultured *in vitro* to expand their population size followed by a transplantation *in vivo* so that the cells may help in overcoming a pathological condition. In order to be able to monitor the behavior of the cells after transplantation

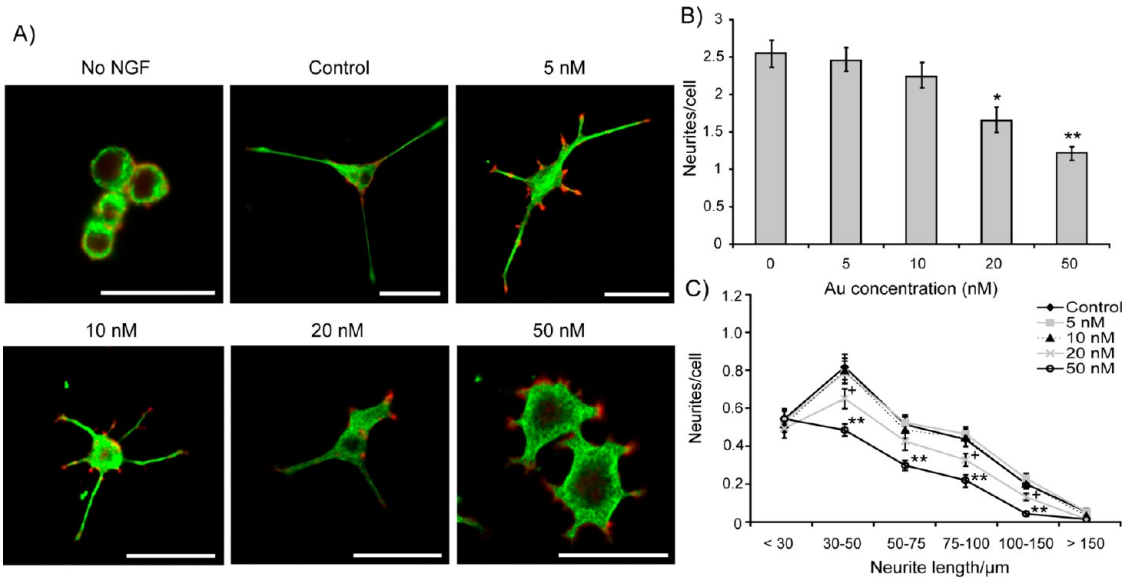

Figure 8. (A) Representative confocal micrographs of PC12 cells incubated with Au NPs for 24 h at the concentration indicated followed by 2 days of NGF exposure, showing α-tubulin (green) and G-actin red) staining. Scale bars: 50 μm. Representative cells not exposed to NGF, control cells exposed only to NGF, and cells incubated with NGF after exposure to Au NPs at 5, 10, 20, or 50 nM are shown. (B) Histograms representing the average number of neurites per cell for NGF-exposed cells incubated with 0, 5, 10, 20, or 50 nM Au NPs for 24 h. Data are expressed as mean ± SEM. When appropriate, the degree of significance when compared with untreated controls cells is indicated (*$p < 0.05$; **$p < 0.01$). (C) Number of neurites of a certain length per cell for NGF-exposed cells incubated with Au NPs for 24 h at 0, 5, 10, 20, or 50 nM. When appropriate, the degree of significance when compared with untreated control cells is indicated ($^{+}p < 0.05$ (20 nM); **$p < 0.01$ (50 nM)).

and the extent of their integration in the host tissue to replace damaged host cells, the cells are often marked with a labeling agent during their time in culture. As organic dyes tend to photobleach and are often not well suited for imaging in deeper tissues and radiotracers also have a limited lifespan and are preferentially excluded because of radiation issues, the use of inorganic NPs such as quantum dots, iron oxide NPs, or Au NPs has gained a lot of interest.[32,54−57] The unique characteristics of these NPs allow to track the fate of the labeled cells *in vivo* using near-infrared fluorescence, magnetic, optical, or photoacoustic imaging. An important consideration in this respect, however, is that the cellular uptake of the NPs may not have any effect on the functionality of the labeled cells, as this might then impede their *in vivo* usefulness. Here, we tested the effect of the PMA-coated Au NPs on the ability of PC12 cells to respond to nerve growth factor (NGF) stimulation by inducing neurite growth. PC12 cells are small, semiadherent cells with typically a near round morphology when cultured under growth conditions (Figure 8A, nNo NGF). However, when the cells are exposed to 100 ng/mL NGF, they respond by rapidly inducing neurite outgrowth, as can be seen in Figure 8A, where control cells and cells labeled with the Au NPs at 5, 10, 20, or 50 nM for 24 h were exposed to NGF for 48 h. The ability of the cells to grow neurites can then easily be quantified (Figure 8B, C) using specialized software, as described in the Materials and Methods section. In order to exclude any effects caused by binding of NGF or nutrients to the nanoparticle surface, NGF was only administered after removal of the NP incubation medium. Furthermore, cells were also exposed to NGF medium that was previously incubated with the Au NPs for 24 h, after which the particles were removed by ultracentrifugation, which did not lead to any effects on outgrowth of PC12 neurites (data not shown).

On the basis of the images and the quantitative data obtained, it can clearly be seen that higher levels of Au NPs (50 nM) significantly impeded cell functionality, impeding both the number of neurites extending per cell (Figure 8B) and the average length of the neurites (Figure 8C). Also at 20 nM, the PMA-coated Au NPs still led to significant reductions in cell functionality despite the lack of a significant effect in any of the previous assays. This finding is supported by previous data and is confirming the work by Pisanic *et al.*,[58] who introduced the PC12 cell model system as a highly sensitive and quantifiable tool to study NP-induced cellular dysfunctions.[25] To date, the effect of Au NPs on stem cell functionality remains elusive, and only sparse data have been obtained so far. Although several studies have described the effect of Au NPs on mesenchymal stem cells, the results are at first glance quite contradictory, as either both adipogenesis and osteogenesis are inhibited,[44,45] adipogenesis is inhibited whereas osteogenesis is stimulated,[46] or neither adipogenesis or osteogenesis is affected.[32] These variations may be due to differences in physicochemical properties of the Au NPs, differences in the labeling conditions used, or the precise type of measurement

that was performed. However, the use of standard differentiation assays followed by qualitative analysis of differentiation capacities that is frequently done to evaluate NP-induced cellular stress does not appear to be well suited to study any NP-mediated effects. Standard differentiation assays as done for mesenchymal stem cells take from up to 7 days to two weeks. That may lead to a significant dilution of intracellular NP contents in time and an associated recovery of the cells when NP levels drop under a significant level. Furthermore, typical differentiation protocols are very stressful for the cells and are often accompanied with high rates of cell death. Because of this, any cells that may already have experienced any stress induced by the NPs are likely to be lost during the differentiation process itself, leaving only those cells that have experienced the least NP-induced effects and, thus, the cells that have taken up the lowest amount of NPs.[59] The rapid induction of neurite outgrowth of PC12 cells, the low associated cell death, and the ease of quantification put forward these cells as an elegant and sensitive model system to study cell–NP interactions.

Defining Nontoxic Au NP Level and the Underlying Cytotoxic Mechanisms. Taking together all the previous data, it was shown that 4 nm diameter PMA-coated Au NPs resulted in direct cytotoxic effects when incubated for 24 h at concentrations of 200 nM or more. Next, a concentration-dependent induction of ROS, reaching significant levels starting from 50 nM Au NPs was also observed. At 100 nM, the induced ROS levels resulted in a significant loss of mitochondrial membrane potential and generated DNA double-strand breaks, the extent of which was likely not enough to result in direct cell death in the time window used in the present study, but may result in severe secondary side-effects at a later stage. The induced oxidative stress also affects cell viability through NFκB pathway activation. Although the induction of oxidative stress is the major cause of cytotoxic effects, it does not account for all cytotoxicity, suggesting that other mechanisms appear to play a role. At concentrations above 50 nM, concentration-dependent effects of the Au NPs on actin and tubulin cytoskeleton and associated signaling were observed. Together with the induction of ROS, the impeded actin-mediated signaling is likely to explain the decreases in cell viability at higher Au NP concentrations. Using the PC12 cell model, which allows for a rapid and quantifiable assessment of cell functionality, it was further observed that the outgrowth of neurites was significantly impeded when cells were incubated at concentrations of 20 nM and higher. In total, no effects at all were observed at concentrations of 10 nM of the NPs. Using inductively coupled plasma spectrometry, it was determined that for C17.2 cells incubated at 10 nM, 6.99×10^5 NPs were taken up per cell (Table 1). Taking into account the total cell population and the total number of particles initially applied to the cells, the cellular uptake efficiency was calculated to be 2.72%. This high number of internalized NPs is in the range of other values reported in the literature[32] and is likely to be more than sufficient to allow most biomedical applications. More data on the minimal amount of Au required to allow photoacoustic imaging of transplanted cells or laser ablation of tumor cells is however needed to verify this.

The present study also offers many exciting future possibilities and future questions to be answered. The multiparametric approach that was used here was shown to offer many advantages compared to common cell viability assays, enabling defining the mechanisms underlying NP toxicity and obtaining a nontoxic level of the NPs tested that was significantly lower than the level found using classical cell viability assays. In the present work, the PMA-coated 4 nm diameter Au NPs were fully characterized and vigorously tested. The data obtained here will therefore serve as a comparative tool for future studies, where Au NPs of various sizes, shapes, and coatings can be tested under identical conditions, allowing an in-depth analysis of the respective contribution of any of these parameters on NP toxicity. As different NPs will affect cells by different mechanisms, depending on many factors such as colloidal stability and cellular uptake efficiency, future studies must be carried out to verify whether the observed effects are common for all types of Au NPs or whether certain coatings or NP sizes can be found that reach similar intracellular levels of Au while inducing less negative effects.

CONCLUSIONS

The present work offers a detailed and multiparametric approach to assess cell–NP interactions. The use of multiple and sensitive cell types (each with their specific traits), different incubation concentrations and times, and the various aspects that were studied provides a nice overview of how NPs can interfere with normal cellular homeostasis. The obtained results highlight the importance of using multiple assays to cover a substantial data set on cell–NP interactions, as there are multiple ways of how the particles can interact with cultured cells and these effects are easily overlooked using standard toxicity assays. The results obtained using the previously defined protocol for assessing NP toxicity provide a nice reference point for future comparison of other nanomaterials tested under the same conditions, and the assays themselves may help to establish highly needed standardized protocols for future NP toxicity assessments. Using this multiparametric approach, a concentration of 10 nM of PMA-coated 4 nm diameter Au NPs (leading to 6.99×10^5 NPs/cell) was found not to lead to any significant effects with respect to cell viability, ROS induction, cell morphology, or functionality. Importantly, the final noncytotoxic concentration of 10 nM that was defined

is approximately 10-fold lower than the concentration that was obtained using commonly used cell viability assays (100 nM), further emphasizing the importance of including multiple parameters to evaluate the toxic effects of nanosized materials on cultured cells. As multiple sensitive cell types have been tested, this concentration seems to be a good reference point for any safe cell labeling studies employing Au NPs with similar physicochemical properties. For any specialized or sensitive cell types, minimal cytotoxicity studies should still be obtained, however, in terms of ROS levels, cellular uptake efficiency, and cell-specific capacities to further confirm that this concentration is also safe for the cell type under consideration and to exclude the possibility of Au NPs interacting with a specific cellular pathway. Furthermore, although the current multiparametric methodology focuses on studying parameters that have been found to occur with a large number of different types of inorganic nanomaterials, this is not an exhaustive list of parameters to be studied, as, for instance, the leaching of metal ions should also be addressed for acid-labile NPs. Additionally, specific mechanisms such as immunological effects or the induction of specific pathways by a particular type of NP are not included and must be studied separately. The present work demonstrates the strength of the multiparametric assessment of NP cytotoxicity in view of *in vitro* cell labeling applications and allows a better definition of the nontoxic concentration of NPs as well as provides a reference for future studies employing the same methodology, enabling a direct comparison of different NPs or the effect of size, surface charge, and coating on NP toxicity.

MATERIALS AND METHODS

PMA-Coated Au NP Synthesis. Au NPs with an inorganic core of around 4 nm diameter were synthesized. The synthesis was carried out in organic solvents according to previously reported protocols.[22] The particles were characterized with TEM and UV–vis absorption spectroscopy. The concentration of the particles was calculated from the absorption at the surface plasmon resonance peak of 518 nm with the Beer–Lambert law using an extinction coefficient (ε) value of $8.63 \times 10^6\ M^{-1}\ cm^{-1}$. The Au NPs were transferred to aqueous solutions *via* a polymer coating procedure using poly(isobutylene-alt-maleic anhydride) dodecylamide (25% anhydride–75%C_{12}COOH) and purified by gel electrophoresis and size exclusion chromatography.[60] The buffer was switched to PBS 1× in order to perform the corresponding experiments, and the concentration was adjusted to 2.5 μM *via* ultrafiltration. Full details are given in the Supporting Information.

Dynamic Light Scattering and Electrophoretic Mobility Measurements. The hydrodynamic diameter and surface charge of the PMA-coated Au NPs were measured using a Nanosizer instrument (Malvern, Worcestershire, UK). The Au particles were suspended in phosphate-buffered saline (PBS: 10 mM; pH 7.0), after which the measurements were performed (12 cycles/run) in quadruplicate. The value for the hydrodynamic diameter of the particles is obtained using the intensity scaling. Data are expressed as mean ± standard deviation ($n = 4$).

Cell Culture Conditions. C17.2 neural progenitor cells and PC12 cells are maintained in high-glucose Dulbecco's modified Eagle's medium, supplemented with 10% fetal bovine serum, 5% horse serum, 2 mM L-glutamine, and 1% penicillin/streptomycin (Gibco, Invitrogen, Merelbeke, Belgium). Cells were maintained in a humidified atmosphere at 5% CO_2, and fresh medium was added every other day. C17.2 cells were passaged (1/10) when they reached 90% confluency. PC12 cells were grown in 25 cm^2 cell culture flasks (Corning, Amsterdam, The Netherlands) that were coated with collagen (rat tail collagen type I, Invitrogen, Belgium) and passaged (1/5) when growing in small clumps (approximately 5 cells/clump and reaching 70–80% confluency). Fresh medium was added every other day.

Primary human umbilical vein endothelial cells were obtained from healthy human volunteers. For cultivation, cells were kept in 75 cm^2 cell culture flasks (Corning, Amsterdam, The Netherlands) that were coated with collagen (rat tail collagen type I, Invitrogen, Belgium) prior to cell seeding. The cells were maintained in endothelial cell basal growth medium and growth supplement (Cell Applications, Tebu-Bio, Le Perray en Yvelines, France) and passaged (1/5) after reaching 80–90% confluency. Every other day, fresh medium was added.

Cell–Nanoparticle Interaction Studies. The full methodology on cell–nanoparticle interaction studies can be found in the Supporting Information.

Statistical Analysis. All data are expressed as mean ± SEM unless indicated otherwise and analyzed using one-way analysis of variance (ANOVA). When comparing the different conditions to the same control group, the Dunnett *post hoc* analysis method was used. In all cases, the degree of significance is indicated when appropriate (*$p < 0.05$; **$p < 0.01$; ***$p < 0.001$).

Conflict of Interest: The authors declare no competing financial interest.

Acknowledgment. The authors thank Dr. Aldo Ferrari (ETH Zürich) for his kind donation of HUVEC cells. S.J.S. is a postdoctoral fellow of the FWO Vlaanderen. Financial support by the Ghent University Special Research Fund (NB Photonics) is gratefully acknowledged. Parts of this work were supported by the European Commission (project Nandiatream to W.J.P.).

Supporting Information Available: Full methodology and additional data are available free of charge *via* the Internet at http://pubs.acs.org.

REFERENCES AND NOTES

1. Liu, Y. F.; Wang, H. F. Nanomedicine–Nanotechnology Tackles Tumours. *Nat. Nanotechnol.* **2007**, *2*, 20–21.
2. Halas, N. J. The Photonic Nanomedicine Revolution: Let the Human Side of Nanotechnology Emerge. *Nanomedicine (London)* **2009**, *4*, 369–371.
3. Seigneuric, R.; Markey, L.; Nuyten, D. S. A.; Dubernet, C.; Evelo, C. T. A.; Finot, E.; Garrido, C. From Nanotechnology to Nanomedicine: Applications to Cancer Research. *Curr. Mol. Med.* **2010**, *10*, 640–652.
4. Rajanikant, G. K.; Teli, M. K.; Mutalik, S. Nanotechnology and Nanomedicine: Going Small Means Aiming Big. *Curr. Pharm. Des.* **2010**, *16*, 1882–1892.
5. Bellare, J. R. Nanotechnology and Nanomedicine for Healthcare: Challenges in Translating Innovations from Bench to Bedside. *J. Biomed. Nanotechnol.* **2011**, *7*, 36–37.
6. Oberdorster, G. Safety Assessment for Nanotechnology and Nanomedicine: Concepts of Nanotoxicology. *J. Intern. Med.* **2010**, *267*, 89–105.
7. Tee, G.; Choi, W. I.; Kim, J. Y.; Kang, C.; Byeon, C. C.; Kim, Y. H. Tumor Regression *in Vivo* by Photothermal Therapy Based on Gold-Nanorod-Loaded, Functional Nanocarriers. *ACS Nano* **2011**, *5*, 1995–2003.
8. Hamad-Schifferli, K.; Wijaya, A.; Schaffer, S. B.; Pallares, I. G. Selective Release of Multiple DNA Oligonucleotides from Gold Nanorods. *ACS Nano* **2009**, *3*, 80–86.

9. Kopelman, R.; Popovtzer, R.; Agrawal, A.; Kotov, N. A.; Popovtzer, A.; Balter, J.; Carey, T. E. Targeted Gold Nanoparticles Enable Molecular CT Imaging of Cancer. *Nano Lett.* **2008**, *8*, 4593–4596.
10. Daniel, M. C.; Astruc, D. Gold Nanoparticles: Assembly, Supramolecular Chemistry, Quantum-Size-Related Properties, and Applications toward Biology, Catalysis, and Nanotechnology. *Chem. Rev.* **2004**, *104*, 293–346.
11. Patra, H. K.; Banerjee, S.; Chaudhuri, U.; Lahiri, P.; Dasgupta, A. K. Cell Selective Response to Gold Nanoparticles. *Nanomed. Nanotechnol.* **2007**, *3*, 111–119.
12. Tarantola, M.; Pietuch, A.; Schneider, D.; Rother, J.; Sunnick, E.; Rosman, C.; Pierrat, S.; Sonnichsen, C.; Wegener, J.; Janshoff, A. Toxicity of Gold-Nanoparticles: Synergistic Effects of Shape and Surface Functionalization on Micromotility of Epithelial Cells. *Nanotoxicology* **2010**, *5*, 254–268.
13. Zhang, X. D.; Wu, H. Y.; Wu, D.; Wang, Y. Y.; Chang, J. H.; Zhai, Z. B.; Meng, A. M.; Liu, P. X.; Zhang, L. A.; Fan, F. Y. Toxicologic Effects of Gold Nanoparticles in Vivo by Different Administration Routes. *Int. J. Nanomed.* **2010**, *5*, 771–781.
14. Simon, U.; Jahnen-Dechent, W. Function Follows Form: Shape Complementarity and Nanoparticle Toxicity. *Nanomedicine (London)* **2008**, *3*, 601–603.
15. Chan, W. C. W.; Chithrani, B. D.; Ghazani, A. A. Determining the Size and Shape Dependence of Gold Nanoparticle Uptake into Mammalian Cells. *Nano Lett.* **2006**, *6*, 662–668.
16. Chithrani, B. D.; Chan, W. C. W. Elucidating the Mechanism of Cellular Uptake and Removal of Protein-Coated Gold Nanoparticles of Different Sizes and Shapes. *Nano Lett.* **2007**, *7*, 1542–1550.
17. Alkilany, A. M.; Nagaria, P. K.; Hexel, C. R.; Shaw, T. J.; Murphy, C. J.; Wyatt, M. D. Cellular Uptake and Cytotoxicity of Gold Nanorods: Molecular Origin of Cytotoxicity and Surface Effects. *Small* **2009**, *5*, 701–708.
18. Chen, C. Y.; Qiu, Y.; Liu, Y.; Wang, L. M.; Xu, L. G.; Bai, R.; Ji, Y. L.; Wu, X. C.; Zhao, Y. L.; Li, Y. F. Surface Chemistry and Aspect Ratio Mediated Cellular Uptake of Au Nanorods. *Biomaterials* **2010**, *31*, 7606–7619.
19. Lehmann, A. D.; Parak, W. J.; Zhang, F.; Ali, Z.; Rocker, C.; Nienhaus, G. U.; Gehr, P.; Rothen-Rutishauser, B. Fluorescent-Magnetic Hybrid Nanoparticles Induce a Dose-Dependent Increase in Proinflammatory Response in Lung Cells in Vitro Correlated with Intracellular Localization. *Small* **2010**, *6*, 753–762.
20. Monteiro-Riviere, N. A.; Inman, A. O.; Zhang, L. W. Limitations and Relative Utility of Screening Assays to Assess Engineered Nanoparticle Toxicity in a Human Cell Line. *Toxicol. Appl. Pharmacol.* **2009**, *234*, 222–235.
21. Soenen, S. J.; Rivera Gil, P.; Montenegro, J.-M.; Parak, W. G. J.; De Smedt, S. C.; Braeckmans, K. Cellular Toxicity of Inorganic Nanoparticles: Common Aspects and Guidelines for Improved Nanotoxicity Evaluation. *Nano Today* **2011**, *6*, 446–465.
22. Parak, W. G. J.; Lin, C. A. J.; Sperling, R. A.; Li, J. K.; Yang, T. Y.; Li, P. Y.; Zanella, M.; Chang, W. H. Design of an Amphiphilic Polymer for Nanoparticle Coating and Functionalization. *Small* **2008**, *4*, 334–341.
23. Parak, W. J.; Harakeh, S.; Abdel-Massih, R. M.; Rivera Gil, P.; Sperling, R. A.; Meinhardt, A.; Niedwiecki, A.; Rath, M.; Baydoun, E. The Effect of PEG-Coated Gold Nanoparticles on the Anti-Proliferative Potential of Specific Nutrient Synergy. *Nanotoxicology* **2010**, *4*, 177–185.
24. Soenen, S. J.; Himmelreich, U.; Nuytten, N.; Pisanic, T. R., 2nd; Ferrari, A.; De Cuyper, M. Intracellular Nanoparticle Coating Stability Determines Nanoparticle Diagnostics Efficacy and Cell Functionality. *Small* **2010**, *6*, 2136–45.
25. Soenen, S. J.; Himmelreich, U.; Nuytten, N.; De Cuyper, M. Cytotoxic Effects of Iron Oxide Nanoparticles and Implications for Safety in Cell Labelling. *Biomaterials* **2011**, *32*, 195–205.
26. Ghandehari, H.; Arnida; Malugin, A. Cellular Uptake and Toxicity of Gold Nanoparticles in Prostate Cancer Cells: A Comparative Study of Rods and Spheres. *J. Appl. Toxicol.* **2010**, *30*, 212–217.
27. Li, J. J.; Hartono, D.; Ong, C. N.; Bay, B. H.; Yung, L. Y. L. Autophagy and Oxidative Stress Associated with Gold Nanoparticles. *Biomaterials* **2010**, *31*, 5996–6003.
28. Raoof, M.; Corr, S. J.; Kaluarachchi, W. D.; Massey, K. L.; Briggs, K.; Zhu, C.; Cheney, M. A.; Wilson, L. J.; Curley, S. A. Stability of Antibody-Conjugated Gold Nanoparticles in the Endolysosomal Nanoenvironment: Implications for Noninvasive Radiofrequency-Based Cancer Therapy. *Nanomedicine* **2012**, DOI: 10.1016/j.nano.2012.02.001.
29. Brandenberger, C.; Muhlfeld, C.; Ali, Z.; Lenz, A. G.; Schmid, O.; Parak, W. J.; Gehr, P.; Rothen-Rutishauser, B. Quantitative Evaluation of Cellular Uptake and Trafficking of Plain and Polyethylene Glycol-Coated Gold Nanoparticles. *Small* **2010**, *6*, 1669–1678.
30. Brust, M.; Nativo, P.; Prior, I. A. Uptake and Intracellular Fate of Surface-Modified Gold Nanoparticles. *ACS Nano* **2008**, *2*, 1639–1644.
31. Soenen, S. J.; Vercauteren, D.; Braeckmans, K.; Noppe, W.; De Smedt, S.; De Cuyper, M. Stable Long-Term Intracellular Labelling with Fluorescently Tagged Cationic Magnetoliposomes. *ChemBioChem* **2009**, *10*, 257–67.
32. Suggs, L. J.; Ricles, L. R., L. M.; Nam, S. Y.; Sokolov, K.; Emelianov, S. Y. Function of Mesenchymal Stem Cells Following Loading of Gold Nanotracers. *Int. J. Nanomed.* **2011**, *6*, 407–416.
33. Kumar, A.; Ma, H.; Zhang, X.; Huang, K.; Jin, S.; Liu, J.; Wei, T.; Cao, W.; Zou, G.; Liang, X. J. Gold Nanoparticles Functionalized with Therapeutic and Targeted Peptides for Cancer Treatment. *Biomaterials* **2012**, *33*, 1180–9.
34. Zhang, X. D.; Wu, D.; Shen, X.; Liu, P. X.; Fan, F. Y.; Fan, S. J. PEGylated Dendrimer-Entrapped Gold Nanoparticles for in Vivo Blood Pool and Tumor Imaging by Computed Tomography. *Biomaterials* **2012**, *33*, 1107–1119.
35. Pernodet, N.; Fang, X. H.; Sun, Y.; Bakhtina, A.; Ramakrishnan, A.; Sokolov, J.; Ulman, A.; Rafailovich, M. Adverse Effects of Citrate/Gold Nanoparticles on Human Dermal Fibroblasts. *Small* **2006**, *2*, 766–773.
36. Mironava, T.; Hadjiargyrou, M.; Simon, M.; Jurukovski, V.; Rafailovich, M. H. Gold Nanoparticles Cellular Toxicity and Recovery: Effect of Size, Concentration and Exposure Time. *Nanotoxicology* **2010**, *4*, 120–137.
37. Soenen, S. J.; Illyes, E.; Vercauteren, D.; Braeckmans, K.; Majer, Z.; De Smedt, S. C.; De Cuyper, M. The Role of Nanoparticle Concentration-Dependent Induction of Cellular Stress in the Internalization of Non-Toxic Cationic Magnetoliposomes. *Biomaterials* **2009**, *30*, 6803–6813.
38. Soenen, S. J.; Nuytten, N.; De Meyer, S. F.; De Smedt, S. C.; De Cuyper, M. High Intracellular Iron Oxide Nanoparticle Concentrations Affect Cellular Cytoskeleton and Focal Adhesion Kinase-Mediated Signaling. *Small* **2010**, *6*, 832–842.
39. Guan, J. L. Role of Focal Adhesion Kinase in Integrin Signaling. *Int. J. Biochem. Cell B* **1997**, *29*, 1085–1096.
40. Krishna, O. D.; Jha, A. K.; Jia, X.; Kiick, K. L. Integrin-Mediated Adhesion and Proliferation of Human MSCs Elicited by a Hydroxyproline-Lacking, Collagen-Like Peptide. *Biomaterials* **2011**, *32*, 6412–6424.
41. Chen, C. S.; Pirone, D. M.; Liu, W. F.; Ruiz, S. A.; Gao, L.; Raghavan, S.; Lemmon, C. A.; Romer, L. H. An Inhibitory Role for FAK in Regulating Proliferation: A Link Between Limited Adhesion and RhoA-ROCK Signaling. *J. Cell Biol.* **2006**, *174*, 277–288.
42. Bryant, P.; Zheng, Q. X.; Pumiglia, K. Focal Adhesion Kinase Controls Cellular Levels of p27/Kip1 and p21/Cip1 through Skp-2-Dependent and -Independent Mechanisms. *Mol. Cell. Biol.* **2006**, *26*, 4201–4213.
43. Snyder, E. Y.; Deitcher, D. L.; Walsh, C.; Arnoldaldea, S.; Hartwieg, E. A.; Cepko, C. L. Multipotent Neural Cell-Lines Can Engraft and Participate in Development of Mouse Cerebellum. *Cell* **1992**, *68*, 33–51.
44. Li, W. T.; Fan, J. H.; Hung, W. I.; Yeh, J. M. Biocompatibility Study of Gold Nanoparticles to Human Cells. *13th Int. Conf. Biomed. Eng.* **2009**, *23*, 870–873.
45. Li, W. T.; Fan, J. H.; Hung, W. I.; Chen, C. P.; Yeh, J. M. Cytotoxicity and Differentiation Effects of Gold Nanoparticles

to Human Bone Marrow Mesenchymal Stem Cells. *Biomed. Eng.: Appl. Bas. C* **2011**, *23*, 141–152.
46. Zhang, J. C.; Yi, C. Q.; Liu, D. D.; Fong, C. C.; Yang, M. S. Gold Nanoparticles Promote Osteogenic Differentiation of Mesenchymal Stem Cells through p38 MAPK Pathway. *ACS Nano* **2010**, *4*, 6439–6448.
47. Min, B. H.; Choi, K. H.; Choi, B. H.; Park, S. R.; Kim, B. J. The Chondrogenic Differentiation of Mesenchymal Stem Cells on an Extracellular Matrix Scaffold Derived from Porcine Chondrocytes. *Biomaterials* **2010**, *31*, 5355–5365.
48. Nel, A.; Xia, T.; Madler, L.; Li, N. Toxic Potential of Materials at the Nanolevel. *Science* **2006**, *311*, 622–627.
49. Nel, A. E.; Madler, L.; Velegol, D.; Xia, T.; Hoek, E. M. V.; Somasundaran, P.; Klaessig, F.; Castranova, V.; Thompson, M. Understanding Biophysicochemical Interactions at the Nano-bio Interface. *Nat. Mater.* **2009**, *8*, 543–557.
50. Soenen, S. J.; Brisson, A. R.; De Cuyper, M. Addressing the Problem of Cationic Lipid-Mediated Toxicity: The Magnetoliposome Model. *Biomaterials* **2009**, *30*, 3691–701.
51. Diaz, B.; Sanchez-Espinel, C.; Arruebo, M.; Faro, J.; de Miguel, E.; Magadan, S.; Yague, C.; Fernandez-Pacheco, R.; Ibarra, M. R.; Santamaria, J.; *et al*. Assessing Methods for Blood Cell Cytotoxic Responses to Inorganic Nanoparticles and Nanoparticle Aggregates. *Small* **2008**, *4*, 2025–2034.
52. Koike, M.; Yutoku, Y.; Koike, A. Accumulation of p21 Proteins at DNA Damage Sites Independent of p53 and Core NHEJ Factors Following Irradiation. *Biochem. Biophys. Res. Commun.* **2011**, *412*, 39–43.
53. Wright, C. J.; Agboke, F.; Muthu, M.; Michaelis, K. A.; Mundy, M. A.; La, P.; Yang, G.; Dennery, P. A. Nuclear Factor-kappa B (NF-kappa B) Inhibitory Protein I kappa B beta Determines Apoptotic Cell Death following Exposure to Oxidative Stress. *J. Biol. Chem.* **2012**, *287*, 6230–6239.
54. Simon, S. M.; Voura, E. B.; Jaiswal, J. K.; Mattoussi, H. Tracking Metastatic Tumor Cell Extravasation with Quantum Dot Nanocrystals and Fluorescence Emission-Scanning Microscopy. *Nat. Med.* **2004**, *10*, 993–998.
55. Soenen, S. J.; Vande Velde, G.; Ketkar-Atre, A.; Himmelreich, U.; De Cuyper, M. Magnetoliposomes as Magnetic Resonance Imaging Contrast Agents. *Wires Nanomed. Nanobiol.* **2011**, *3*, 197–211.
56. Alivisatos, A. P.; Parak, W. J.; Boudreau, R.; Le Gros, M.; Gerion, D.; Zanchet, D.; Micheel, C. M.; Williams, S. C.; Larabell, C. Cell Motility and Metastatic Potential Studies Based on Quantum Dot Imaging of Phagokinetic Tracks. *Adv. Mater.* **2002**, *14*, 882–885.
57. Dubertret, B.; Skourides, P.; Norris, D. J.; Noireaux, V.; Brivanlou, A. H.; Libchaber, A. In Vivo Imaging of Quantum Dots Encapsulated in Phospholipid Micelles. *Science* **2002**, *298*, 1759–1762.
58. Pisanic, T. R.; Blackwell, J. D.; Shubayev, V. I.; Finones, R. R.; Jin, S. Nanotoxicity of Iron Oxide Nanoparticle Internalization in Growing Neurons. *Biomaterials* **2007**, *28*, 2572–2581.
59. Soenen, S. J.; De Cuyper, M. Assessing Cytotoxicity of (Iron Oxide-Based) Nanoparticles: An Overview of Different Methods Exemplified with Cationic Magnetoliposomes. *Contrast Media Mol. Imaging* **2009**, *4*, 207–219.
60. Parak, W. J.; Sperling, R. A.; Liedl, T.; Duhr, S.; Kudera, S.; Zanella, M.; Lin, C. A. J.; Chang, W. H.; Braun, D. Size Determination of (Bio)Conjugated Water-Soluble Colloidal Nanoparticles: A Comparison of Different Techniques. *J. Phys. Chem. C* **2007**, *111*, 11552–11559.